

# ADAPTIVE HYBRID LEVEL-SET/FRONT-TRACKING FOR DROP FORMATION

**Millena M. Villar, mmvillar@mecanica.ufu.br**

Universidade Federal de Uberlândia, FEMEC/UFU, Av. João naves de Ávila 2121, Uberlândia-MG, Brasil

**Alexandre M. Roma, roma@ime.usp.br**

Universidade de São Paulo, IME/USP-SP, Rua do Matão, 1010 - Cidade Universitária, São Paulo - SP, Brasil

**Aristeu da Silveira-Neto, aristeus@mecanica.ufu.br**

Universidade Federal de Uberlândia, FEMEC/UFU, Av. João naves de Ávila 2121, Uberlândia-MG, Brasil

**Abstract.** *An adaptive hybrid level-set/front-tracking method is applied in order to efficiently solve relevant physical scales of multi-phase flows, specifically deformable droplet and the breakup of fluid-fluid interface. Geometric interfacial quantities are computed from front-tracking while the level-set function, which is evaluated fast and to machine precision, is used as a fluid indicator. To solve accurately sharp gradients and flow features adaptive mesh refinements are employed. Using this numerical methodology is possible to simulate the liquid sheets in which the edge receding and accumulate fluid and an pendant drop formation.*

**Keywords:** *adaptive mesh, front-tracking, level-set, multilevel multigrid, drop formation.*

## 1. INTRODUCTION

Multi-phase flows are a source of numerous nonlinear processes of both scientific and technological relevance. The formation of drops or its impact over a surface is a complex phenomenon which is not easy to predict the distribution of their sizes or to observe the intricate dynamics involved. The phenomenon is also of intrinsic interest because it represents a challenging moving boundary problem. Therefore, the effective numerical simulation of these flows requires both an accurate representation of the singularly supported interfacial forces and of all physically relevant flow quantities and to faithfully capture the disparate scales. The method presented here is able to simulate with accuracy all these quantities. It couples the hybrid level-set/front-tracking (LeFT), the fast and accurate fluid indicator developed in Cenicerós and Roma (2005), and the adaptive immersed boundary (IB) method first introduced by Roma, *et al.* (1999).

LeFT does an explicit tracking of the interface using the IB method framework and employs a continuous level-set function as a fluid indicator. The interfacial tension and the geometric quantities are evaluated from the tracked interface while the level set function is used to update the material quantities. Thus, the method retains one of the advantages of front-tracking (accurate evaluation of interfacial quantities) and at the same time benefits from a continuous, geometry-based fluid indicator, the level-set function. Moreover, this signed distance function is updated only locally, in a thin neighborhood of the interface, at optimal computational cost and is computed to machine precision for a piecewise linear representation of the interface. Here, we also use a hybrid Lagrangian/Eulerian approach due to Shin, *et al.* (2005) to evaluate the tension force. This hybrid force formulation combined with the accurate fluid indicator leads to an unprecedented reduction of spurious currents.

In addition, a semi-implicit time discretization which stably handles the non-linear viscous term explicitly is adopted. As proposed by Ascher *et al.*, (1995), the IMEX (Implicit-Explicit Method) method with some simple modifications assure the time step being restricted only by a linear CFL constraint ( $\Delta t = O(\Delta x)$ ). This efficient semi-implicit time discretization based on IMEX Method is employed along with centered finite differences for the discretization in space. Special multilevel-multigrid methods are applied to solve the linear systems arising from the convection-diffusion equation and from the pressure-correction Poisson equation.

The paper is organized as follows. Section 2 gives a brief introduction to the mathematical model, presenting LeFT method and the hybrid interfacial force adopted. The numerical method is presented in Section 3. In Section 4, two physically relevant numerical examples are presented.

## 2. LEVEL-SET/FRONT-TRACKING METHOD

Consider a single fluid interface separating two incompressible fluids of constant but possibly different densities and viscosities and in the presence of surface tension. In this method the interface or immersed boundary is explicitly tracked and the level set function  $\phi$  is used as a fluid indicator. The motion equation for both fluid and interface  $X(\alpha, t)$ , where  $\alpha$  is a Lagrangian parameter, is given by:

$$\rho(\phi)[\mathbf{u}_t + (\mathbf{u} \cdot \nabla)\mathbf{u}] = \nabla \cdot [\mu(\phi)(\nabla\mathbf{u} + \nabla\mathbf{u}^\dagger)] - \nabla\mathbf{p} + \rho(\phi)\mathbf{g} + \mathbf{f}_H, \quad (1)$$

$$\nabla \cdot \mathbf{u} = 0, \quad (2)$$

$$\mathbf{X}_t(\alpha, t) = \int_{\Omega} \mathbf{u}(\mathbf{x})\delta_h(\mathbf{x} - \mathbf{X}(\alpha, t)) d\mathbf{x}, \quad (3)$$

where  $\phi > 0$  for one of the fluids,  $\phi < 0$  for the other,  $\phi = 0$  along the interface between the two phases and is computed directly but locally using a fast algorithm for signed distance. Here,  $\mathbf{u}$ ,  $p$ ,  $\mathbf{g}$ , and  $\mathbf{f}_H$  are the velocity field, the pressure, the gravitational acceleration, and the surface tension force respectively. The  $\delta$ -distribution in (3) is replaced by mollified function  $\delta_h$  as done originally by Peskin (1977), where  $\delta_h(\mathbf{x}) = d_h(x)d_h(y)$  with

$$d_h(\xi) = \begin{cases} 0.5 [1 + \cos(\frac{\pi}{h} \xi)]/h & \text{for } |\xi| \leq h, \\ 0 & \text{for } |\xi| > h, \end{cases} \quad (4)$$

where  $h = 2\Delta x$ , and here is assumed that  $\Delta x = \Delta y$ .

With the level-set function defined, is possible to obtain the material quantities, given by:

$$\rho(\phi) = \rho_1 + (\rho_2 - \rho_1)H_h(\phi), \quad (5)$$

$$\mu(\phi) = \mu_1 + (\mu_2 - \mu_1)H_h(\phi), \quad (6)$$

where  $\rho_1, \rho_2$  and  $\mu_1, \mu_2$  are the constant densities and viscosities of the bulk phases, respectively, and  $H_h(\phi)$  is a mollified Heaviside function defined by

$$H_h(\xi) = \begin{cases} 0, & \text{for } \xi < -h \\ 0.5 [1 + \xi/h + \sin(\frac{\pi}{h} \xi)/\pi], & \text{for } |\xi| \leq h \\ 1, & \text{for } \xi > h. \end{cases} \quad (7)$$

The hybrid surface tension force  $\mathbf{f}_H$  as proposed by Shin, *et al.* (2005) is briefly shown here, where  $\mathbf{f}_H$  is given by the spread of normal ( $\mathbf{n}$ ) and the lagrangian surface tension force ( $\mathbf{f}_L$ ), such that

$$\mathbf{f}_H(\mathbf{x}) = \sigma\kappa_L(\mathbf{x})\nabla H_h(\phi(\mathbf{x})) \quad (8)$$

$$\kappa_L(\mathbf{x}) = \frac{1}{\sigma} \frac{\mathbf{f}_L(\mathbf{x}) \cdot \hat{\mathbf{n}}_L(\mathbf{x})}{\hat{\mathbf{n}}_L(\mathbf{x}) \cdot \hat{\mathbf{n}}_L(\mathbf{x})}. \quad (9)$$

where  $\kappa$  is the curvature mean,  $\sigma$  is the surface tension, and,

$$\mathbf{f}_L(\mathbf{x}) = \sigma \int_{\Gamma} \kappa(\alpha)\hat{\mathbf{n}}(\alpha)\delta(\mathbf{x} - \mathbf{X}(\alpha))|\mathbf{X}_\alpha(\alpha)| d\alpha, \quad (10)$$

$$\hat{\mathbf{n}}_L(\mathbf{x}) = \int_{\Gamma} \hat{\mathbf{n}}(\alpha)\delta(\mathbf{x} - \mathbf{X}(\alpha))|\mathbf{X}_\alpha(\alpha)| d\alpha. \quad (11)$$

### 3. NUMERICAL METHOD

As said before a hybrid adaptive method is applied, which means that qualities from both front-tracking and level-set method are employed, and by the fact that adaptivity is introduced in space and time through dynamic control of the lagrangian markers and through Eulerian refinement, and trough an adaptive, robust second order semi-implicit temporal discretization (Ceniceros *et al.*, 2009).

A semi-implicit time discretization is based on a second order IMEX schemes (Ascher *et al.*, 1995) with some modifications employed by Badalassi *et al.* (2003) and detailed too in Villar *et al.* (2006).

With the IMEX schemes is possible to obtain a family time discretization, which is applied to Navier-Stokes equation and initially described by:

$$\begin{aligned} \frac{\rho(\phi)}{\Delta t} \left[ (\gamma + \frac{1}{2})\mathbf{u}^{n+1} - 2\gamma\mathbf{u}^n + (\gamma - \frac{1}{2})\mathbf{u}^{n-1} \right] &= (\gamma + 1)f(\mathbf{u}^n) - \gamma f(\mathbf{u}^{n-1}) \\ &+ \mu \left[ \gamma + \frac{c}{2}g(\mathbf{u}^{n+1}) + (1 - \gamma - c)g(\mathbf{u}^n) + \frac{c}{2}g(\mathbf{u}^{n-1}) \right] - \nabla p^{n+1} + \rho(\phi)\mathbf{g}, \end{aligned} \quad (12)$$

where  $f(\mathbf{u})$  represents the advective term and  $g(\mathbf{u})$  the diffusive term.  $\gamma$  and  $c$  are constants with which is possible to obtain the SBDF (semi-backward difference formula), CNAB (Crank Nicolson Adans Bashforth), MCNAB (modified Crank Nicolson Adans Bashforth) and CNLF (Crank Nicolson Leap Frog) Methods.

The equation (12) is rewritten to use here the modifications proposed by Badalassi *et al.* (2003) and Euler Method in the first time step, such that

$$\frac{\rho(\phi)}{\Delta t}(\alpha_2 \mathbf{u}^{n+1} + \alpha_1 \mathbf{u}^n + \alpha_0 \mathbf{u}^{n-1}) = b_1 g(\mathbf{u}^n) + b_0 g(\mathbf{u}^{n-1}) + \lambda \left[ \left( \gamma + \frac{c}{2} \right) \nabla^2 \mathbf{u}^{n+1} + (1 - \gamma - c) \nabla^2 \mathbf{u}^n + \frac{c}{2} \nabla^2 \mathbf{u}^{n-1} \right] - \nabla p^{n+1} + \rho^{n+1}(\phi) \mathbf{g}, \quad (13)$$

where  $\lambda = |\mu|_\infty$ , and  $\alpha_0, \alpha_1, \alpha_2, b_0, b_1$  again are constants that allow the user to decide which IMEX schemes apply. Doing this is necessary to complete the motion equation, and the  $g(\mathbf{u})$  function is not necessarily composed only by advective terms, but either by surface tension term and diffusive term.

$$g(\mathbf{u}) = -\lambda \nabla^2 \mathbf{u} + \nabla \cdot \left[ \mu (\nabla \mathbf{u} + \nabla \mathbf{u}^T) \right] - \mathbf{u} \cdot \nabla \mathbf{u} + \mathbf{f}_H \quad (14)$$

Now is possible to define each constant in agreement to the IMEX scheme desired, being known that the time-step is constant. For SBDF method  $(\gamma, c) = (1, 0)$ , MCNAB method  $(\gamma, c) = (\frac{1}{2}, \frac{1}{8})$ , CNAB method  $(\gamma, c) = (\frac{1}{2}, 0)$ , CNLF method  $(\gamma, c) = (0, 1)$  and for both  $\alpha_2 = \gamma + \frac{1}{2}, \alpha_1 = -2\gamma, \alpha_0 = \gamma - \frac{1}{2}, b_1 = \gamma + 1, b_0 = -\gamma$ . In the first time-step the Euler Method is applied which leads  $(\gamma, c) = (\frac{1}{2}, 0)$  and  $\alpha_2 = 1, \alpha_1 = -1, \alpha_0 = 0, b_1 = 1, b_0 = 0$ .

A fractional-step projection method is applied to the Navier-Stokes equations, resulting a scheme which is second-order accurate for the velocities and at least first-order for the pressure. In practice, the solution of Eqs. (1)-(2) is computed in three steps by a projection method specially designed for composite grids. The following development assumes that the pressure and other scalar functions are placed at the centers of the computational cells, while velocity and other vector function components are placed at cell edges. First, in the *parabolic step*, one must solve, for a provisional velocity  $\mathbf{u}^*$ , the implicit parabolic equation

$$\frac{\rho^{n+1,0}(\phi)}{\Delta t}(\alpha_2 \mathbf{u}^{*n+1} + \alpha_1 \mathbf{u}^n + \alpha_0 \mathbf{u}^{n-1}) = b_1 g(\mathbf{u}^n) + b_0 g(\mathbf{u}^{n-1}) + \lambda \left[ \left( \gamma + \frac{c}{2} \right) \nabla^2 \mathbf{u}^{*n+1} + (1 - \gamma - c) \nabla^2 \mathbf{u}^n + \frac{c}{2} \nabla^2 \mathbf{u}^{n-1} \right] - \nabla p^{n+1,0} + \rho^{n+1,0}(\phi) \mathbf{g}, \quad (15)$$

where  $p^{n+1,0}$  and  $\rho^{n+1,0}$  are given approximations of the pressure and of the density at  $t = t^{n+1}$ , respectively. Second, in the *elliptic step*, where must solve the pressure-correction Poisson equation

$$\nabla \cdot \left( \frac{1}{\rho} \nabla q^{n+1} \right) = \frac{\alpha_2}{\Delta t} \nabla \cdot \mathbf{u}^*, \quad (16)$$

with homogeneous boundary conditions. In the third step, to complete the projection, the provisional velocity field  $\mathbf{u}^*$  is decomposed using the pressure correction obtained

$$\mathbf{u}^{n+1} = \mathbf{u}^* - \frac{\Delta t}{\alpha_2} \frac{\nabla q^{n+1}}{\rho^{n+1,0}}, \quad (17)$$

given as a result  $\mathbf{u}^{n+1}$ , a discretely divergence-free vector field defined on the entire composite grid. This step is referred to as the *decomposition step*.

Another intrinsic problem of front-tracking method applied to multi-phase flows comes from the excessive marker (particle) clustering. To overcome this difficulties Cenicerros and Roma (2004) propose to select a tangential velocity of the interface markers to control their distribution at all times, and the markers move only with the normal velocity of the fluid. Thus 3 is modified by:

$$\mathbf{X}_t(\alpha, t) = \int_{\Omega} \mathbf{u}(\mathbf{x}) \delta_h(\mathbf{x} - \mathbf{X}(\alpha, t)) d\mathbf{x} + U_A(\alpha, t) \hat{\mathbf{t}}, \quad (18)$$

where  $U_A(\alpha, t)$  is arbitrary defined by

$$U_A(\alpha, t) = -U_T(\alpha, t) + \int_0^\alpha (s_\alpha \kappa U_N - \langle s_\alpha \kappa U_N \rangle) d\alpha', \quad (19)$$

where  $U_T = \hat{\mathbf{t}} \cdot \int_{\Omega} \mathbf{u}(\mathbf{x}) \delta_h(\mathbf{x} - \mathbf{X}(\alpha, t)) d\mathbf{x}$ ,  $U_N = \hat{\mathbf{n}} \cdot \int_{\Omega} \mathbf{u}(\mathbf{x}) \delta_h(\mathbf{x} - \mathbf{X}(\alpha, t)) d\mathbf{x}$ ,  $s_\alpha = \sqrt{X_\alpha^2 + Y_\alpha^2}$  is the arc-length metric,  $\kappa$  is the mean curvature, and  $\langle \cdot \rangle$  stands for the spatial mean over one spatial period. It is important to note that the evolution of the interface followed by its regularization is done once more by IMEX scheme.

### 3.1 Adaptive Mesh Refinement

The existence of local phenomena and the need for more grid points to accurately capture them suggest the application of local mesh refinement techniques. The AMR developed by Berger and coworkers (Berger and Olinger (1984) and Berger and Colella (1989)) and extended to the elastic interfaces by Roma *et al.* (1999) is based on a collection of logically rectangular meshes that make up the coarse grid; refinements cover a subset of the domain and use smaller rectangular grid patches. These finer patches can be recursively nested until a given level of accuracy is attained. For this case special multilevel-multigrid methods are applied to solve the linear systems arising from the convection-diffusion equation and from the pressure-correction Poisson equation. An example of adaptive mesh used here is presented in Fig. 1.

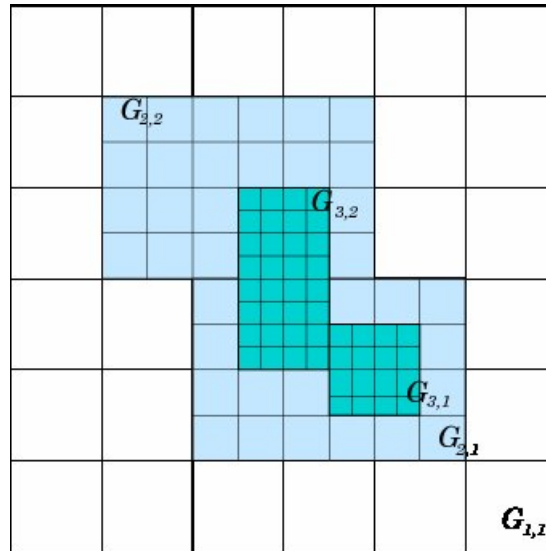


Figure 1: An example of structured adaptive mesh

A staggered (composite) grid, i.e., pressure and other scalar variables are placed at the centers of the computational cells, the first component of vector variables are placed at the middle of the vertical edges, and the second component are placed in the middle of the horizontal ones. The discretization of the Laplacian, gradient and divergence differential operators are performed by standard, cell-centered second order stencils.

## 4. RESULTS

Two tests are presented to verify the capabilities of the proposed adaptive hybrid method in the formation of growth waves and the breakup of drop. One analyze the instabilities that lead to the growth waves and later the breakup in the middle of the sheet and not at the edge as shown by Song and Tryggvason (1999). The last test focus on process of breakup and the formation of the primary drop.

### 4.1 Fluid-Film

During the drop formation process, in many atomizers, a thin liquid sheet that eventually breaks up into drops is formed. Although, before the disintegration of the liquid sheets the edge receding and accumulate fluid. The breakup of filaments has been studied by a large number of authors, such as Lozano *et al.* (1998) and Song and Tryggvason (1999) but today is still very complex to understand the physics that governs the growth waves and the breakup. Here two-dimensional simulation try to explore the vorticity filed formation during the receding and accumulate fluid process to explain its formation.

Many study shows that the edge of the sheet is pulled back by surface tension, forming a thick blob. The speed at which the edge is pulled back depends primarily on the Ohnesorge number ( $Oh = \frac{\mu_d}{(\rho_d d \sigma)^{0.5}}$ ), which is the ratio of viscous forces to surface force, and to a lesser degree on the properties of the extern fluid. Three values of Ohnesorge are reproduced here  $Oh = 0,98$ ,  $Oh = 0,098$ ,  $Oh = 0,0098$ , in an  $\Omega = [0, 1] \times [0, 4]$  domain and  $32 \times 128L3$  adaptive mesh. The initial length of the sheet is 3,7 and its thickness is 0,15. For this simulation the SBDF method was applied.

The Figure 2 presents the evolution of vorticity field at  $Oh = 0,0098$ , which admit low viscosity effects leading the formation of symmetric waves that propagate along the sheet, away from the blob. These instabilities will create a primary drop and many satellite drops. The origin of these instabilities comes from in flexional profile velocity, where the inflection point is on the interface. This inflection allow the formation of the Kelvin-Helmholtz instability that generates

a pressure jump with a bigger external pressure than in the internal region. In the other hand, a negative curvature takes place and creates a restoring force out of the interface. Those three mechanisms (pressure jump, surface tension force and vorticity) assure a condition to amplify the instability leading to the necking.

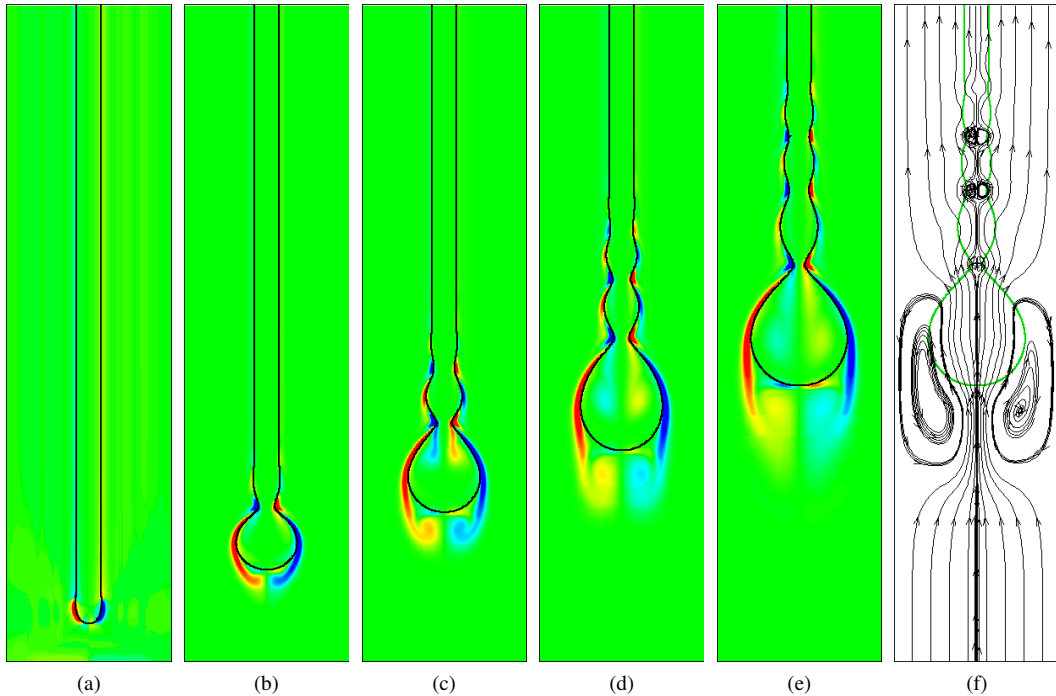


Figure 2: Evolution of the sheet boundary overlapped by vorticity field at  $Oh = 0,0098$ . (a)  $t = 0,39s$ , (b)  $t = 50,75$ , (c)  $t = 101,5s$ , (d)  $t = 152,25s$ , (e)  $t = 203s$  e (f) stream lines at  $t = 203s$

The Figure 3 shows the pressure field and the velocity graphic at  $Oh = 0,98$  for  $t = 30s$ . In this case is possible to note the smooth inflexional velocity graphic (Fig. 3b) which doesn't lead to necking. A steep profile is observed in  $Oh = 0,098$  and  $Oh = 0,0098$ . The Figs. 4 - 5 shows again the pressure field and the vertical velocity taken in the position indicated by the dashed line. At  $Oh = 0,0098$  the steep inflexional profile is noted in the first initial time-steps for  $t = 3,9s$ .

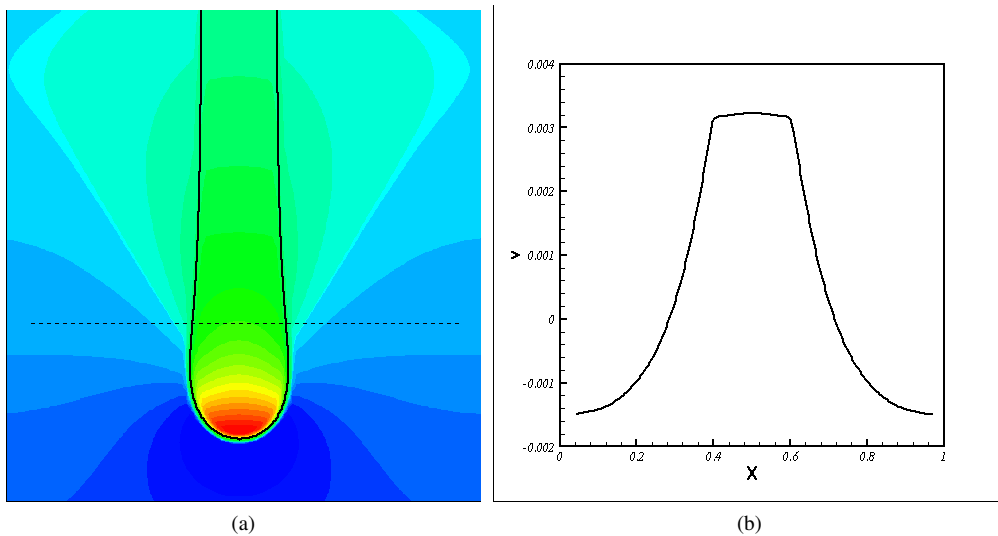


Figure 3: (a) Pressure field at  $Oh = 0,98$  and  $t = 30s$ , (b) Velocity graphic taken at the dashed line position.

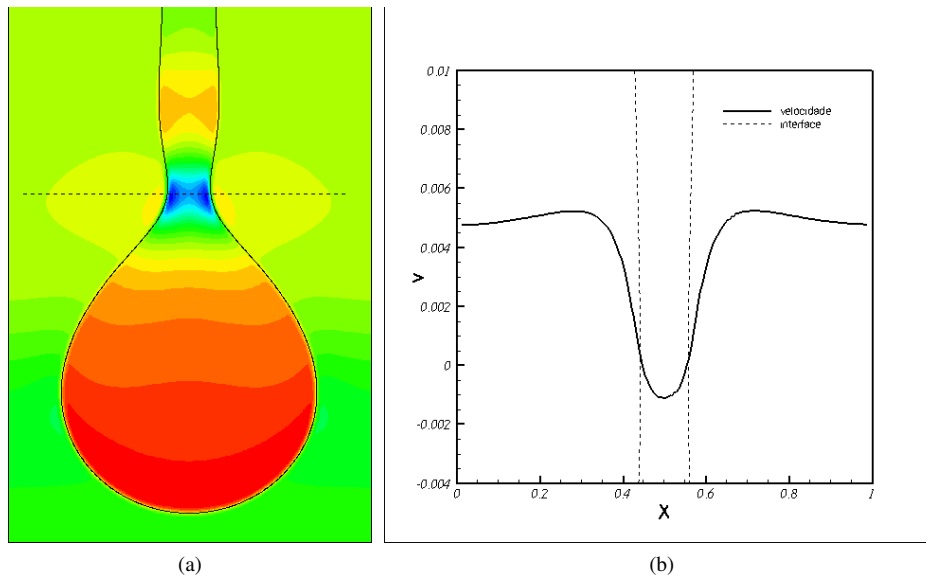


Figure 4: (a) Pressure field at  $Oh = 0,098$  and  $t = 300s$ , (b) Velocity graphic taken at the dashed line position.

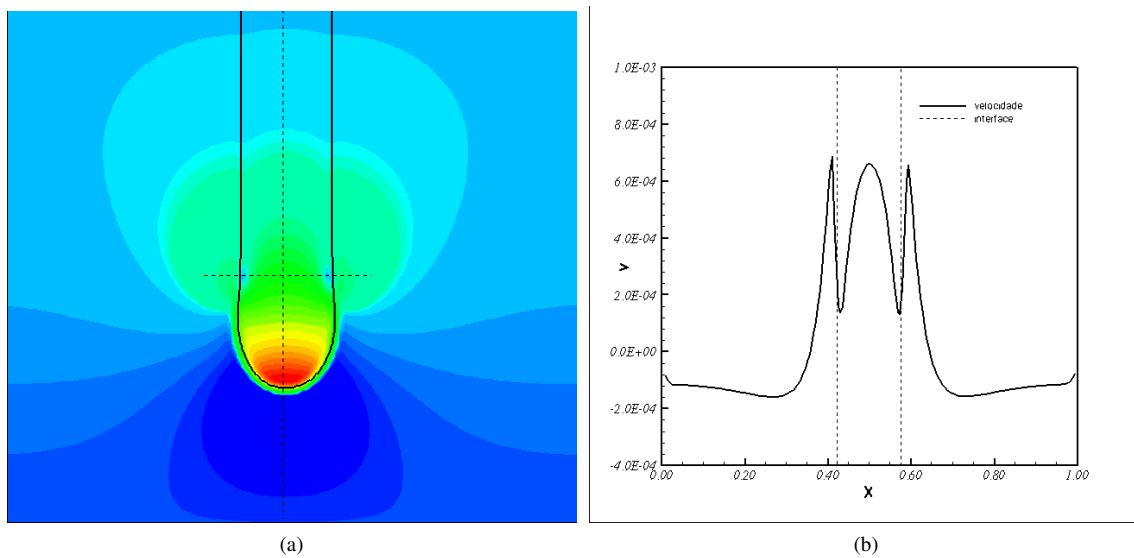


Figure 5: (a) Pressure field at  $Oh = 0,0098$  and  $t = 3,9s$ , (b) Velocity graphic taken at the dashed line position.

## 4.2 Pendant drop

The dynamics of the growth and detachment of drops from a capillary tube or a nozzle into ambient fluids is a challenging task to numerical simulation due to high ratio of physical properties, the formation of extremely sharp regions in the process of breakup and the presence of high curvature (Davison and Cooper-White, 2006; Yildirim *et al.*, 2005 and Wilkes *et al.*, 1999).

To simulate the pendant drop, consider a drop growing downward in a gas phase from a cylindrical nozzle with internal diameter  $2a$  and external diameter  $4a$  as shown in Fig. 6. The relevant parameters include gravity, surface tension, and viscous effects. Here is defined the Bond number and the Weber number. The Bond number represents the ratio of gravity to capillary forces ( $Bo = \rho_1 g r_0^2 / \sigma$ ). The Weber number compares inertia and capillarity forces and it is based on the influx velocity  $V$  ( $We = \rho_1 V^2 r_0 / \sigma$ ). A velocity profile linear is assumed at the end of the nozzle located at the top boundary of numerical box  $v = V(1 - x/r_0)$  for  $x < r_0$  and  $v = 0$  for  $x > r_0$ , where  $r_0 = a = 1 \cdot 10^{-3}m$ .

The simulation is reported on  $32 \times 64L5$  grid, with  $Bo = 1,20$ ,  $Fr = 1,74$ ,  $Oh = 5,91 \cdot 10^{-2}$ ,  $\rho_1/\rho_2 = 1000$ ,  $\mu_1/\mu_2 = 333$ , and  $Q = 4,12 \cdot 10^{-7}m^3/s$ . For this case the MCNAB method is applied, which assure larger time-step and stability. The evolution of fragmentation process is shown in the Fig. 7.

An important issue in the drop formation process is the flow field inside a drop. During the period that a drop grows, recirculating toroidal edges are created in the vicinity of the drop surface. The liquid elements, tend to flow toward the

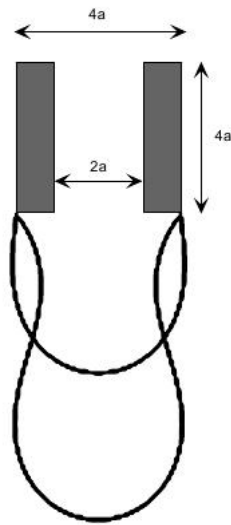


Figure 6: Schematic drop shape.

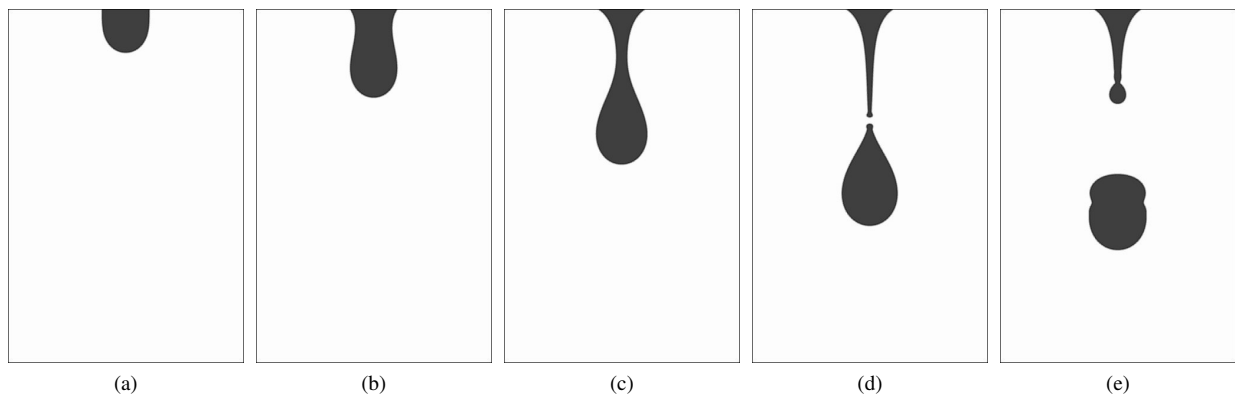


Figure 7: Evolution of density in time on  $32 \times 64L5$  grid.

apex of the drop along its axis of symmetry flowing tangentially into annular space, resulting in recirculations within the drop. So the eddies disappear and the fluid motion is essentially in the downward direction (Zhang, 1999). In Fig. 8 is possible to note these toroidal recirculations through the vorticity field. When the flow rate is low or moderate, after the first breakup, the thread rolls up rapidly due to the unbalanced capillary force and breaks again generating a satellite droplet. By contrast, at  $Q > 3,33 \cdot 10^{-7} m^3/s$  after its first breakup, the threads rolls and coalesces with the liquid cone without secondary breakup and satellite drop generation.

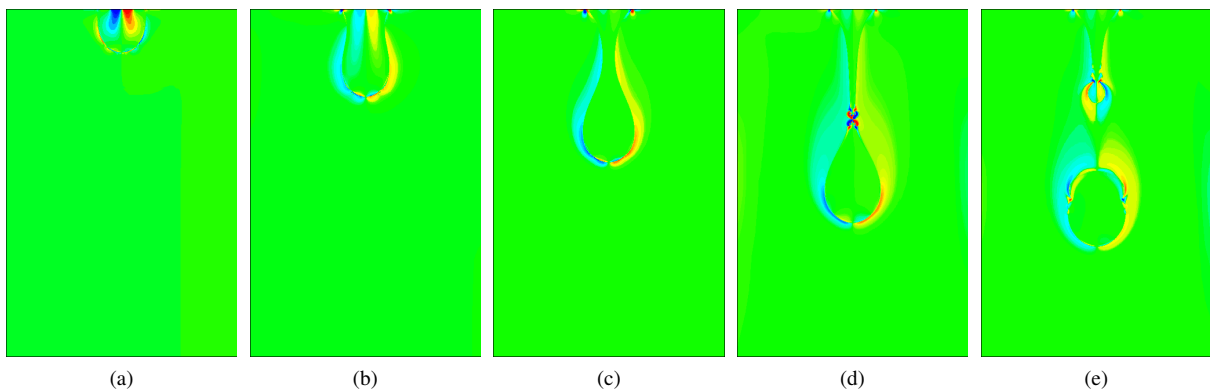


Figure 8: Evolution of vorticity field in time on  $32 \times 64L5$  grid.

Many existant numerical methods are not conservative when the breakup process occur. The adaptive hybrid method presented here, allow to quantify and reduce, without excessive computational cost, the mass loss in the breakup process. The graphic plotted in Fig. 9 shows the evolution of flux mass per  $m/s$  in time on a two refinement levels. For  $32 \times 64L4$  the mass loss was 0,99% while the  $32 \times 64L5$  presents just 0,025%.

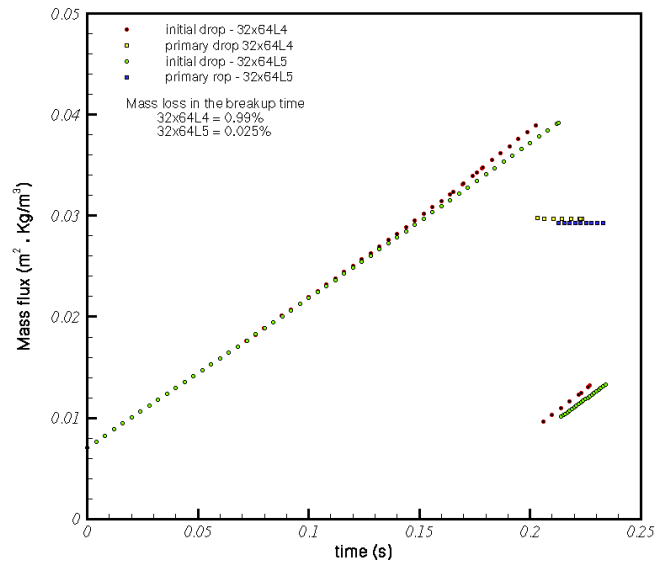


Figure 9: Evolution of flux max per  $m/s$ .

## 5. CONCLUSIONS

In this work the performance of the adaptive hybrid level-set/front-tracking method was illustrated through the simulations of deformable fluid-fluid interface interactions. The dynamic adaptation presented occur both in the lagrangian markers and Eulerian mesh refinement which increase locally the resolution of the fluid solver with a sequence of nested, progressively finer refinement levels.

It allows to simulate with a high level of precision and low cost, the Kelvin-Helmholtz instabilities formation on a film-fluid and the breakup process on a drop. In both cases were employed adaptive mesh refinement, second-order discretization in space and time and semi-implicit temporal discretization. In the first case was possible to verify the inflexional profile that creates the waves propagation and helps in the creation of necking process. The last case use front-tracking methodology to simulate a breakup process drop with minimum mass loss about 0,025%. The observed features of the elastic fluid-fluid interface deformation were well reproduced at  $Q = 4,12 \cdot 10^{-7} m^3/s$ .

## 6. ACKNOWLEDGMENTS

The authors would like to thank the Conselho Nacional de Pesquisa e Desenvolvimento of Brasil (CNPq), Petrobras and FAPEMIG for financial support.

## 7. REFERENCES

- Ascher, U. M., Ruuth, S. J. and Wetton, B. T. R., 1995, "Implicit-Explicit Methods for Time-Dependent PDE'S", SIAM J. Numer. Anal., Vol.32, pp. 797 - 823.
- Badalassi, V. E., Cenicerros, H. D. and Banerjee, S., 2003, "Computation of Multiphase Systems with Phase Field Models", J. Comput. Phys., Vol.190, pp. 371 - 397.
- Berger, M.J. and Colella, P.,1989, "Local Adaptive Mesh Refinement for Shock Hydrodynamics", J. Comput. Phys. Vol.82, pp. 64 - 84.
- Berger, M. J, and Rigoutsos, I, 1991, " An Algorithm for Point Clustering and Grid Generation", IEEE Transactions on Systems, Man, and Cybernetics, Vol. 21, pp. 1278 -1286.

- Berger, M. J. and Olinger, J., 1984, "Adaptive Mesh Refinement for Hyperbolic Partial Differential Equations". *Journal of Computational Physics*, Vol. 53, pp 484-512.
- Ceniceros, H. D., Roma, A. M., Silveira-Neto, A. and Villar, M. M., 2009, "A Robust, Fully Adaptive Hybrid Level-Set/Front-Tracking Method for Two-phase Flows with an Accurate Surface Tension Computation", submitted at *Communication in Computational Physics*.
- Ceniceros, H. D. and Roma, A. M., 2005, "A Multi-Phase Flow Method with a Fast, Geometry-Based Fluid Indicator". *Journal of Computational Physics*, Vol.205, pp. 391 – 400.
- Ceniceros, H. D., and Roma, A. M., 2004, "Study of Long-Time Dynamics of a Viscous Vortex Sheet with a Fully Adaptive non-Stiff Method", *Phys. Fluids*, Vol. 16, pp. 4285 –4318.
- Davidson, M. R. and Cooper-White, J. J., 2006, "Pendant Drop Formation of Shear-Thinning and Yield" *Stress Fluids, Applied Mathematical Modeling*, Vol.30, pp. 1392 - 1405.
- Lozano, A., Olivares, A. G. and Dopazo, C., 1998, "The Instability Growth Leading to a Liquid Sheet Breakup", *Phys. Fluids*, Vol.10, p. 2188– 2197
- Roma, A. M, Peskin, C. S. and Berger, M. J., 1999, "An Adaptive Version of the Immersed Boundary Method", *J. Comput. Phys.* Vol.153, pp. 509– 534.
- Peskin, C. S., 1977, "Numerical Analysis of Blood Flow in the Heart", *J. Comput. Phys*, Vol.25, pp. 220 - 252.
- Shin, S., Abdel-Khalik, S.I, Daru, V. and Juric, D., 2005, "Accurate Representation of Surface Tension Using the Level Contour Reconstruction Method", *J. Comput. Phys.* Vol. 203, pp. 493–516.
- Song, M. and Tryggvason, G., 1999, "The Formation of Thick Borders on an Initially Stationary Fluid Sheet", *Physics of Fluids*, Vol. 11, No. 9, 2487– 2493.
- Villar, M. M, Roma, A. M, Silveira-Neto, A. and ceniceros, H. D., 2006, "An Adaptive Second-Order Projection Method For Unsteady Flows", *Iberian Latin American Congress on Computational Methods in Engineering*.
- Wilkes, E. D., Phillips, S. D. and Basaran, O. A., 1999, "Computational and Experimental Analysis of Dynamics of drop Formation", *Physics of Fluids*, Vol. 11, No. 12, 3577-3598
- Yildirim, O. E., Xu, Q. and Basaran, O. A., 2005, "Analysis of the Drop Weight Method", *Physics of Fluids*, Vol. 17, No. 13, pp. 062107– 062107.
- Zhang, X., 1999, "Dynamics of Growth and Breakup of Viscous Pendant Drops into Air", *Journal of Colloid and Interface Science*, Vol. 212, pp. 107 - 122.

## 8. Responsibility notice

The authors are the only responsible for the printed material included in this paper